

# Single-photon detectors for optical quantum information applications

Robert H. Hadfield

**The past decade has seen a dramatic increase in interest in new single-photon detector technologies. A major cause of this trend has undoubtedly been the push towards optical quantum information applications such as quantum key distribution. These new applications place extreme demands on detector performance that go beyond the capabilities of established single-photon detectors. There has been considerable effort to improve conventional photon-counting detectors and to transform new device concepts into workable technologies for optical quantum information applications. This Review aims to highlight the significant recent progress made in improving single-photon detector technologies, and the impact that these developments will have on quantum optics and quantum information science.**

One of Einstein's key contributions to modern science was to recognize that light is fundamentally composed of individual packets of energy, now referred to as photons<sup>1,2</sup>. The energy of a single photon in the visible or near-infrared range is around  $10^{-19}$  J. A single-photon detector is an extremely sensitive device capable of registering these quantum objects. Single-photon detectors now support and enable a host of applications at the frontiers of science and engineering. Conventional single-photon detectors are based on photomultipliers and avalanche photodiodes, and are used in a wide range of time-correlated single-photon counting (TCSPC) applications<sup>3</sup>. However, the major driver for single-photon detector development has been the rapidly expanding interest in optical quantum information (QI) applications<sup>4</sup>. Quantum information technologies use individual quantum objects (such as photons) to encode and manipulate information<sup>5</sup>, and promise to have a dramatic technological impact in the twenty-first century<sup>6</sup>. The most mature of these innovations is quantum key distribution (QKD)<sup>7,8</sup>, the most secure form of communication yet devised, and is now at the point of becoming commercially viable. Perhaps the most ambitious photonic QI application is linear optical quantum computing (LOQC)<sup>9-11</sup> — a scalable paradigm for QI processing and computation. LOQC remains a distant but tantalizing objective, and significant efforts have been mobilized worldwide towards this goal. A major reason that advanced QI technologies such as LOQC are so difficult to realize is the stringent demands these applications place on optical components such as single-photon detectors<sup>12</sup>. Significant improvements are required in terms of their signal-to-noise ratio, detection efficiency, spectral range and ability to resolve photon number (the number of photons reaching the detector simultaneously). Scientists and engineers around the world have taken up this challenge. Their efforts have led to considerable improvements in conventional single-photon detectors and to the emergence of new photon-counting technologies.

## Quantifying the performance of single-photon detectors

The performance of a single-photon detector should be assessed<sup>8,13</sup> in terms of its spectral range, dead time, dark count rate, detection efficiency, timing jitter and ability to resolve photon number. We will consider these characteristics in detail, in particular with reference to the requirements of different optical QI applications. Spectral range, dead time, dark count rate, detection efficiency and timing jitter are all important general benchmarks for single-photon detectors, and the ability to resolve photon number is required

in advanced QI protocols<sup>10,11</sup>. We will outline accurate measurement strategies for characterizing single-photon detectors and discuss an appropriate 'figure of merit' for quantifying detector performance.

**Spectral range.** A photon counter is only sensitive over a certain spectral range determined by its constituent materials. The operating wavelength of interest depends on the particular application. For free-space optical applications (either bench-top quantum optics experiments<sup>13</sup> or line-of-sight QKD through the atmosphere<sup>8</sup>) visible or near-infrared wavelengths are used to exploit the best commercially available detectors. Losses in optical fibre are lowest at a wavelength of 1,550 nm, making this wavelength a clear choice for long distance QKD in optical fibres<sup>8</sup>. Other advanced optical components such as on-chip waveguides are also tailored to telecommunications wavelengths. There is therefore considerable interest in the field of QI in telecommunications-wavelength detectors.

**Dead time.** The detector 'dead time' or recovery time,  $\tau$ , is the time interval that follows the absorption of a photon, during which the detector is unable to reliably register a second photon. The factors influencing  $\tau$  depend strongly on the detector type. In many cases, the measured value of  $\tau$  is that of the bias circuit or the counting electronics, rather than the detector element itself. In semiconductor single-photon detectors,  $\tau$  is deliberately lengthened to suppress afterpulsing, the spontaneous retriggering of the detector after an initial detection event. The dead time limits the maximum count rate of the detector but not the clock rate of the experiment, which can be much higher because TCSPC experiments are typically operated in the regime where the number of detected photons per clock cycle is much less than one.

**Dark count rate.** Most practical detector technologies have a finite probability of recording false counts, known as dark counts, dark noise or dark current, which arise either due to the materials properties of the detector, the biasing conditions or the susceptibility to external noise. In practical applications, the dark count rate of interest,  $D$ , is that measured with the detector embedded in the experiment — dark count measurements of completely shielded detectors can give unrealistic values that are of little help or guidance to potential users.  $D$  is usually given by a rate in hertz, but can be mitigated by gating or time-stamping the detection events. The minimum time interval for gating or time-stamping is set by the timing jitter of the detector.

**Box 1 | Measurement of the detection efficiency,  $\eta$**

Measurement of  $\eta$ , the probability of registering a count if a photon arrives at the detector, can be achieved through two distinct methods.

**Calibrated light source method**

This method (Fig. B1a) relies on calibrating a light source with a power meter and then attenuating the output heavily to determine the incident power  $P$ . The number of incident photons per second is given by  $R_{\text{incident}} = P\lambda/hc$ , where  $\lambda$  is the wavelength and  $hc/\lambda$  is the energy per photon. One would expect that measurements using either pulsed or continuous wave (CW) sources should give the same reading. If, however, the detector recovery is affected by even a weak photon flux (as in the case of many semiconductor detectors where photon absorption affects the occupancy of low-lying trap states), then a pulsed measurement, in which the frequency  $f$  is lower than  $1/\tau$  (where  $\tau$  is the detector dead time), is the more reliable of the two measurements. Moreover, detector saturation or afterpulsing is easier to detect in a pulsed measurement. However, it is important to note that optical power meters are often only accurately calibrated for CW input power.

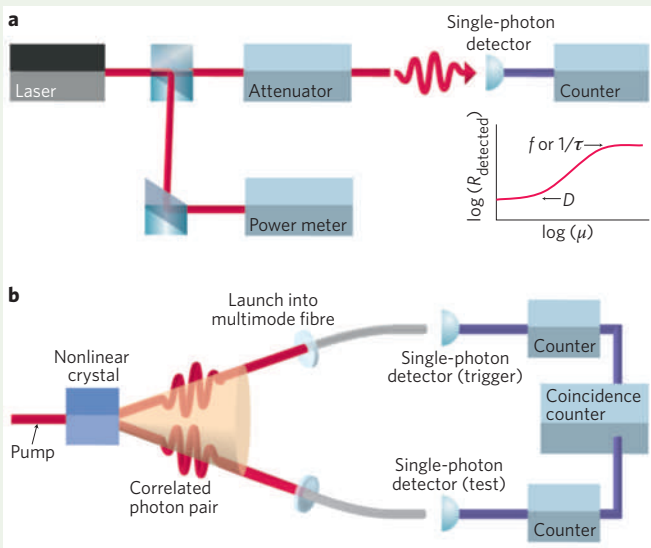


**Figure B1 | Determination of single-photon detector efficiency.**

**a**, Calibrated laser method. A continuous wave or pulsed laser is measured using a calibrated power meter. A series of calibrated attenuators are then used to reduce the photon flux  $\mu$  to less than one photon per time interval. The count rate of the detector  $R_{\text{detected}}$  is recorded over a range of values of  $\mu$ . Typically,  $R_{\text{detected}}(\mu)$  will be of the form shown in the inset. In the continuous-wave case,  $R_{\text{detected}}$  will saturate at the inverse of the detector (or counter) recovery time,  $\tau$ . In the pulsed case, saturation should occur at the repetition frequency of the laser,  $f$ . At low values of  $\mu$ , the residual count rate is due to dark counts in the detector. At intermediate values of  $\mu$ , the signature of a single-photon detector is that  $R_{\text{detected}}$  is proportional to  $\mu$ . **b**, Correlated photon method. This method avoids the need for a calibrated power meter. A pair of correlated photons is produced from spontaneous parametric down-conversion source. The signal and idler photons are routed to the test and trigger detectors, then the respective count rates — including coincidences between the two channels — are recorded. The detection efficiency of the test detector channel is given by the coincidence rate divided by the count rate at the trigger detector.

**Measurement using a CW source.** For the case of a CW measurement of  $\eta$ , the fundamental time interval is set by  $\tau$ . The mean photon number per time interval,  $\mu$ , is

$$\mu = R_{\text{incident}} \tau$$

For a Poissonian light source in the limit of  $\mu\eta \ll 1$ , the count rate of an ideal detector is

$$R_{\text{detected}} = \frac{1}{\tau} (1 - \exp(-\mu\eta)) \approx \frac{\mu\eta}{\tau}$$

The true count rate due to actual photodetection events,  $R'_{\text{detected}}$ , can be derived by correcting for the separately measured dark count rate  $D$  and the dead time  $\tau$ , giving

$$R'_{\text{detected}} = \left( \frac{R_{\text{detected}}}{1 - R_{\text{detected}}\tau} - \frac{D}{1 - D\tau} \right)$$

The detection efficiency is therefore

$$\eta = \frac{R'_{\text{detected}}}{R_{\text{incident}}} = \tau \left( \frac{R_{\text{detected}}}{1 - R_{\text{detected}}\tau} - \frac{D}{1 - D\tau} \right) / \mu$$

The parameters  $\eta$ ,  $\mu$  and  $\tau$  can be determined by analysing a plot of  $R_{\text{detected}}$  against the photon flux per time interval,  $\mu$  (Fig. B1a, inset). At low numbers of detected photons ( $\mu\eta \ll 1$ ) the signature of single-photon sensitivity is that  $R_{\text{detected}} \propto \mu$ , but a detector triggered by a two-photon event would give  $R_{\text{detected}} \propto \mu^2$ .

**Measurement using a pulsed source.** For a pulsed source of frequency  $f \ll 1/\tau$  and a mean photon number per pulse  $\mu$ ,

$$R_{\text{incident}} = \mu f$$

$$R_{\text{detected}} = f(1 - \exp(-\mu\eta)) \approx \mu\eta f$$

One would therefore expect the detector count rate to saturate under high photon flux at the clock rate of the source. In this case, the detection efficiency is given by

$$\eta = \frac{R_{\text{detected}}}{R_{\text{incident}}} = \left( \frac{R_{\text{detected}}}{1 - R_{\text{detected}}\tau} - \frac{D}{1 - D\tau} \right) / \mu f$$

**Correlated photon method**

The correlated photon method (Fig. B1b) uses a source of correlated photons to characterize the detector<sup>14,15</sup>. Remarkably, this elegant technique requires no calibrated power meter. Photons from the pump laser of frequency  $\omega_p$  are converted into signal and idler photons of frequency  $\omega_s$  and  $\omega_i$ , respectively, by spontaneous parametric down-conversion, which conserves energy and momentum such that  $\omega_p = \omega_s + \omega_i$ . The signal and idler photons are directed to the test and trigger detectors. Coincidences between the two detector channels are recorded.  $N$  is the number of photon pairs emitted in the counting period. The counts in the test and trigger detector are given by  $N_1 = \eta_1 N$  and  $N_2 = \eta_2 N$ , respectively, and the total coincidence counts are given by  $N_{\text{coinc}} = \eta_1 \eta_2 N$ . The detection efficiency of the test detector is therefore  $\eta_1 = N_{\text{coinc}}/N_2$ , which is independent of the efficiency of the trigger channel. This technique, however, only gives the overall efficiency of the test detector channel, which is problematic for small (<100  $\mu\text{m}$  diameter) detectors.

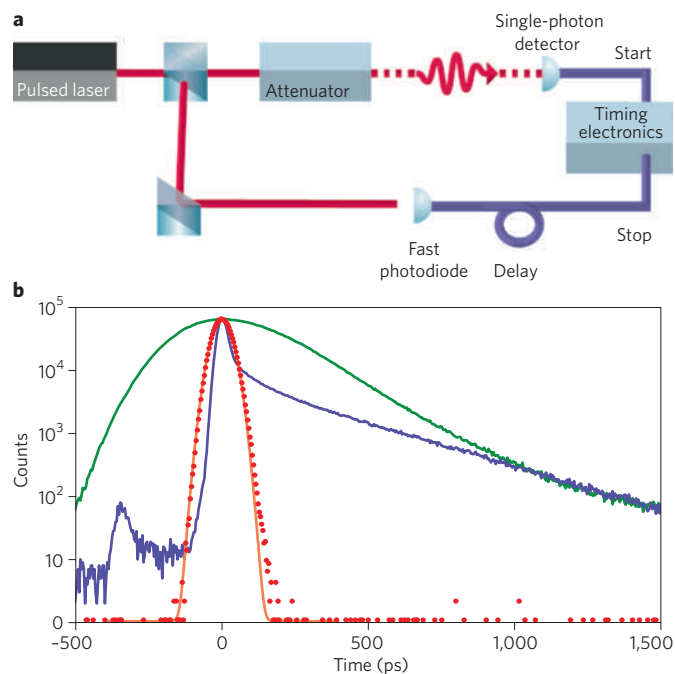


**Figure 1 | Measurement of timing jitter.** **a**, The timing jitter of a single-photon detector is the variation in delay between the absorption of a photon and the generation of an output electrical pulse. To measure the timing jitter accurately, a picosecond pulsed laser and high-resolution timing electronics are required to ensure that the dominant jitter is that of the detector. A count on the single-photon detector triggers the ‘start’ for the timing electronics, and the delayed clock pulse from the laser signals the ‘stop’. A histogram of start-stop time intervals is accumulated over multiple clock cycles, giving the instrument response of the single-photon detector. **b**, Instrument responses of three types of single-photon detector, measured using a mode-locked Ti:Sapphire laser at 780 nm and picosecond timing electronics. The thick junction Si SPAD (green) has a FWHM response of ~400 ps, the shallow junction SPAD (blue) has a FWHM response of ~40 ps but with a strongly asymmetric instrument response function, and the superconducting nanowire single-photon detector (red) has a FWHM response of 68 ps with a Gaussian shape. Part **b** reproduced with permission from ref. 16, © 2009 AIP.

**Detection efficiency.** The detection efficiency,  $\eta$ , is defined as the overall probability of registering a count if a photon arrives at the detector. In most photon-counting applications a high value of  $\eta$  is certainly desirable, but it is by no means the only practical consideration. The maximum rate at which data can be accumulated in an experiment is governed by both the mean photon number per time interval,  $\mu$ , and the maximum count rate of the detector,  $1/\tau$ . Moreover, signal-to-noise considerations are often the true determining factor as to whether an experiment is feasible. The exception is LOQC<sup>9</sup>, where an extremely high value of  $\eta$  is essential. For scalable LOQC (even with new cluster-state protocols<sup>10,11</sup>), overall optical losses, including collection from the source, cannot fall below a 67% threshold<sup>12</sup>.

Methods of accurately determining  $\eta$  are shown in Box 1, either by using a calibrated light source (Fig. B1a) or correlated photon pairs (Fig. B1b)<sup>14,15</sup>. In the ideal case, the detection efficiency is defined as  $\eta = R_{\text{detected}}/R_{\text{incident}}$ , where  $R_{\text{detected}}$  is the count rate and  $R_{\text{incident}}$  is the photon arrival rate. The intrinsic quantum efficiency of the actual device is not the paramount concern for the user; the practical detection efficiency  $\eta$  must include the optical coupling efficiency to the detector (through free-space optics or optical fibres). The overall

detection efficiency  $\eta$  of a detector channel is therefore the product of coupling losses,  $\eta_{\text{loss}}$ , and the intrinsic quantum efficiency of the detector,  $\eta_{\text{det}}$ , such that  $\eta = \eta_{\text{loss}} \eta_{\text{det}}$ . When  $\eta$  is measured accurately, the dead time  $\tau$  of the detector and the counting electronics must be considered. Furthermore, the measured count rate of the detector,  $R_{\text{detected}}$ , should be corrected for the finite dark count rate of the detector.

**Timing jitter.** This is the variation in the time interval between the absorption of a photon and the generation of an output electrical pulse from the detector. A reliable method of measuring  $\Delta t$  for a single-photon detector is shown in Fig. 1a. The full-width half-maximum (FWHM) of the detector instrument response function provides a benchmark for timing jitter. Many detectors have a non-Gaussian instrument response function, however, and this should be taken into account in any detailed analysis. The maximum clock rate of a photon counting experiment (where the mean detected photon number is given by  $\eta\mu \ll 1$ ) is determined by the timing resolution, and jitter in the source or detector will cause counts to stray into neighbouring clock cycles. Typically, but not always, the detector jitter is dominant. Examples of instrument response functions for three detectors are shown in Fig. 1b<sup>16</sup>.

**Ability to resolve photon number.** Most conventional single-photon detectors can only distinguish between zero or ‘one or more’ photons<sup>10,17</sup>. This binary response means that a multiphoton pulse triggers the same output signal as a single photon. QI protocols require single-photon states, which are difficult to prepare in practice because attenuated laser pulses obey Poissonian statistics; the probability of producing a photon state  $|n\rangle$  is  $P(n) = (\mu^n/n!)e^{-\mu}$ , where  $\mu = \langle n \rangle$  is the mean number of photons per pulse<sup>2</sup>. On-demand single-photon sources for QI applications are a highly active research field. Despite significant progress<sup>18,19</sup>, current single-photon sources are imperfect because the second-order correlation function  $g^{(2)}(0)$  is non-zero, implying residual multiphoton emission, and also because source emission rates are low (that is,  $\mu \ll 1$ ). In QKD, multiphoton states represent a security ‘loophole’ that can be exploited by eavesdroppers. In LOQC<sup>9–11</sup>, efficient detection of all photons is crucial for reducing errors. Photon number resolution has been achieved in two ways (Fig. 2). First, certain single-photon detector types (such as superconducting transition edge sensors) intrinsically produce a pulse proportional to the number of photons absorbed (Fig. 2a)<sup>20</sup>. The second method multiplexes conventional detectors<sup>17</sup>. This can be achieved either by combining the output signals of an array of detectors (spatial multiplexing; Fig. 2b)<sup>21,22</sup> or by splitting the multiphoton pulse via a cascade of beamsplitters and then delaying the signals so that they can be detected sequentially by a single detector (time multiplexing; Fig. 2c)<sup>23</sup>. The fidelity with which an  $n$ -photon state can be recorded scales as  $\eta^n$  — thus, high-efficiency detectors are desirable for these applications. In a multiplexed photon-number-resolving scheme, it is necessary to have a large number of pixels (or time bins)  $N$ , such that  $N \gg n$ , to reduce the possibility that two or more photons were absorbed at any one pixel.

**Figures of merit for single-photon detectors.** The most widely quoted figure of merit for photodetectors is the noise equivalent power (NEP)<sup>24</sup>, and this has proved useful for optical power measurements. For single-photon detectors, the NEP can be given by

$$\frac{h\nu}{\eta} \sqrt{2D}$$

where  $\nu$  is the photon frequency and  $h$  is Planck’s constant. The units of NEP are  $\text{W Hz}^{-1/2}$ , and the lowest possible value of NEP is desirable. However, a typical detector (one that does not resolve photon

number) does not measure optical power. Furthermore, NEP does not take into account the timing performance of the detector, nor does it relate  $D$  and  $\eta$  in a meaningful way for QI experiments. For example, in a QKD experiment, the detector contribution to the quantum-bit error rate (QBER) is the ratio of the dark count rate to the sifted detected photon rate (the detected rate after comparison of the transmission and receiving bases). Furthermore,  $D$  can be reduced by setting the timing window as small as possible. Unless some other factor (the jitter of a single-photon source, for example) has a dominant role, the minimum timing interval is usually limited by the timing jitter of the detector. We can therefore formulate a dimensionless figure of merit that takes all of these factors into consideration, giving

$$H = \eta / (D\Delta t)$$

This is a useful figure not only for QKD but also for a range of TCSPC measurements, both in QI applications and beyond. Better detectors have a higher value of  $H$  at the wavelength of interest.

This section has rigorously considered the characterization of single-photon detectors and devised an appropriate figure of merit for optical QI applications. It is crucial to understand these characteristics when selecting the best detector for a given experiment or application. Established and emerging single-photon detectors are compared through these metrics in Table 1.

### Established single-photon detector technologies

This section reviews the current performance and future prospects of established single-photon detector technologies. In each case, the operating principle, performance, advantages and disadvantages of each detector type are discussed. Performance characteristics are shown in Table 1. New developments and the potential for further improvements in performance are also noted. Short reviews have been given previously elsewhere<sup>10,17,18</sup>, and recent special issues devoted to the topic of photon-counting technologies are also recommended reading<sup>4,25</sup>.

**Photomultiplier tubes.** The most long-established photon-counting technology is the photomultiplier tube (PMT). Single-photon counting in PMTs was demonstrated in 1949<sup>26</sup>, and this development heralded the birth of the field of TCSPC<sup>3,27</sup>. Commercial PMT units are now widely available<sup>28,29</sup>, and there are continued efforts to improve these devices. Photomultiplier tubes offer large active-areas (diameters of >10 mm) and cover the spectral range of 115–1,700 nm, but with large variations in performance.

A basic PMT consists of a vacuum tube with a photocathode for light absorption, from which electrons are liberated through the photoelectric effect (the energy of the incident photon must exceed the work function of the photocathode material). This single- or few-electron photocurrent is then multiplied by a cascade of secondary electron-emissions from dynodes — a series of electrodes, each one biased at a greater positive voltage than the one before — producing a macroscopic current pulse of >10<sup>6</sup> electrons. Traditional PMTs require large operating voltages around the kilovolt-level, and are fragile and expensive. In certain types of PMT, the excess noise of the multiplication process is sufficiently low to allow some discrimination between one or multiple photons. An alternative configuration is the microchannel plate photomultiplier tube, where glass capillaries are fused in parallel and coated with a secondary electron-emitting material to achieve a single continuous dynode under a bias voltage<sup>30</sup>. Microchannel plate PMTs offer improved timing jitter over basic PMTs, down to ~20 ps at FWHM<sup>30</sup>.

Photomultiplier tubes have a maximum efficiency of around 40% at a wavelength of 500 nm in GaAsP photocathodes, and have dark

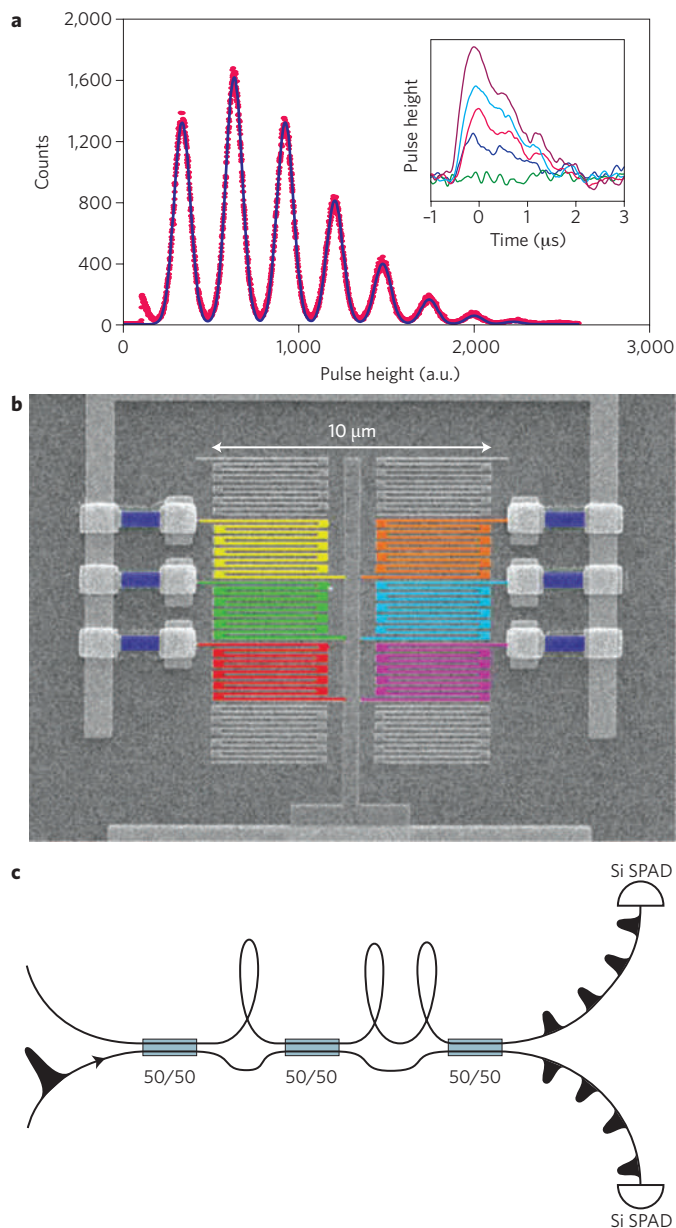


**Figure 2 | Photon number resolution.** Conventional single-photon detectors give a digital response — an output pulse or ‘click’ indicates the arrival of one or more photons. Determining the number of photons in a pulse requires a photon-number-resolving detector. **a**, True photon number resolution. Detectors with true photon number resolution give an output that depends on the number of photons absorbed. The superconducting TES is essentially a microcalorimeter — the height of the pulse is proportional to the number of photons at a given wavelength. The figure shows a TES measurement of Poissonian statistics with a mean photon number per pulse of 2.45 at 1,550 nm. The line shows a plot of best-fit to the data, convolving the Poissonian distribution with the energy resolution of the TES. Shown inset is the TES pulse heights for zero to four photons. **b,c**, Conventional single-photon detectors can be combined through spatial or temporal multiplexing to achieve photon number resolution. In spatial multiplexing (**b**), an array of detector pixels (in this case SNSPDs) are broadly illuminated and read-out in parallel. When several pixels are triggered simultaneously, the output pulses are summed. In temporal multiplexing (**c**), The input optical pulse is split via a network of delayed paths such that each photon can be picked out within the dead time interval of the detector pair. Image in **b** reproduced with permission from ref. 22, © 2008 NPG.

**Table 1 | Comparison of single-photon detectors.**

Detector type	Operation temperature (K)	Detection efficiency, $\eta$	Jitter time, $\Delta t$ (FWHM)	Dark count rate, $D$ (ungated)	Figure of merit	Max. count rate	Resolves photon number?	Class of report
PMT (visible–near-infrared) <sup>31</sup>	300	40% @500 nm	300 ps	100 Hz	$1.33 \times 10^7$	10 MHz	Yes	†
PMT (infrared) <sup>32</sup>	200	2% @1,550 nm	300 ps	200 kHz	$3.33 \times 10^2$	10 MHz	Yes	†
Si SPAD (thick junction) <sup>38</sup>	250	65% @650 nm	400 ps	25 Hz	$6.5 \times 10^7$	10 MHz	No	†
Si SPAD (shallow junction) <sup>41</sup>	250	49% @550 nm	35 ps	25 Hz	$5.6 \times 10^8$	10 MHz	No	†
InGaAs SPAD (gated) <sup>55</sup>	200	10% @1,550 nm	370 ps	91 Hz	$2.97 \times 10^5$	10 kHz	No	‡
InGaAs SPAD (self-differencing) <sup>57</sup>	240	10% @1,550 nm	55 ps	16 kHz	$1.14 \times 10^5$	100 MHz	Yes	‡
Frequency up-conversion <sup>65</sup>	300	9% @1,550 nm	400 ps	13 kHz	$1.7 \times 10^4$	10 MHz	No	‡
Frequency up-conversion <sup>65</sup>	300	2% @1,550 nm	40 ps	20 kHz	$2.5 \times 10^4$	10 MHz	No	‡
VLPC <sup>69</sup>	6	88% @694 nm	—	20 kHz	—	—	Yes	§
VLPC*	6	34% @633 nm	270 ps	7 kHz	$1.83 \times 10^5$	—	Yes	§
TES <sup>76</sup>	0.1	50% @1,550 nm	100 ns	3 Hz	$1.67 \times 10^6$	100 kHz	Yes	‡
TES <sup>20</sup>	0.1	95% @1,550 nm	100 ns	—	—	100 kHz	Yes	§
SNSPD (meander) <sup>90</sup>	3	0.7% @1,550 nm	60 ps	10 Hz	$1.16 \times 10^7$	100 MHz	No	‡
SNSPD (new) <sup>87</sup>	1.5	57% @1,550 nm	30 ps	—	—	1 GHz	No	§
QD (resonant tunnel diode) <sup>96</sup>	4	12% @550 nm	150 ns	$2 \times 10^{-3}$ Hz	$4 \times 10^9$	250 kHz	No	§
QD (field-effect transistor) <sup>93</sup>	4	68% @805 nm	—	—	—	1 Hz	Yes	§

The class of report indicates the conditions under which the detector characteristics were measured; † represents a commercial product specification, ‡ represents the use of the detector in a practical experiment and § represents a measurement of device performance. \*Unpublished data, Burm Baek, NIST, USA, 2009.

count rates as low as 100 Hz (ref. 31). The highest reported count rates are up to 10 MHz, and the typical jitter is 300 ps at FWHM<sup>31</sup>. PMTs are now available at telecommunications wavelengths<sup>31</sup> by cooling an InP/InGaAs photocathode to 200 K. Performance is poor compared with visible-wavelength PMTs, however, with a detection efficiency of 2% at 1,550 nm, a dark count rate of 200 kHz and a jitter of ~300 ps at FWHM. Another important development has been the hybrid photodetector, which combines a photocathode with a low-capacitance avalanche photodiode<sup>33</sup>. Hybrid photodetectors require low bias voltages of around 400 V, offer 46% efficiency at 500 nm, and have a timing jitter of 61 ps at FWHM and ~1 kHz dark count rates<sup>33</sup>.

**Single-photon avalanche photodiodes.** Silicon single-photon avalanche photodiodes (Si SPADs; Fig. 3a,b)<sup>34</sup> are now a well-established alternative to PMTs in laboratory quantum optics experiments<sup>13</sup> and free-space QKD systems. These solid-state devices offer low dark count rates, high detection efficiencies and high count rates in the visible to near-infrared range. The long wavelength cut-off is a result of the semiconductor bandgap of Si. In the UV range, absorption occurs before the photon reaches the detection region.

The SPAD is based on an avalanche photodiode structure (a p–n or p–i–n junction). The diode is reverse-biased above the breakdown voltage, and this is known as Geiger mode operation. Carriers generated by photon absorption undergo avalanche gain, triggering a macroscopic breakdown of the diode junction<sup>35</sup>. To harness this

effect in a practical device, the avalanche must be stopped and the device reset by a quenching circuit<sup>34,36</sup>.

The highest efficiency commercial devices are based on a thick, 180- $\mu\text{m}$ -diameter high-purity silicon absorber combined with an active quenching circuit and cooling in a single practical module<sup>37,38</sup>. These devices offer single-photon sensitivity in the 400–1,000 nm range and achieve a peak efficiency of 65% at ~650 nm (ref. 38). Dark count rates can be as low as 25 Hz (ref. 36) and the timing jitter is typically ~400 ps at FWHM<sup>16</sup> (Fig. 1b). The operating voltage is low at around 400 V. In Si SPADs the afterpulsing probability is low, with quenching times of approximately 50 ns. Although the excess noise of the multiplication process is too high in SPADs to achieve intrinsic photon number resolution, efforts have been made to achieve this indirectly by exploiting timing walk effects<sup>39</sup> or through spatial-<sup>21</sup> or temporal-multiplexing<sup>23</sup> schemes. Photon emission by hot carriers in an avalanche current ('backflash' photons) can potentially be exploited by eavesdroppers in QKD schemes<sup>40</sup>.

A new generation of Si SPAD devices are now available<sup>41</sup>. These are shallow-junction planar devices<sup>42</sup> that have a diameter of 50  $\mu\text{m}$  and require only low operating voltages. The timing is greatly improved to below 40 ps at FWHM (Fig. 1b), but the peak detection efficiency is reduced to 49% at 550 nm.

Silicon SPADs remain an active area of development<sup>43</sup>. Efforts are underway to integrate detector elements directly with quenching circuitry<sup>44</sup>, and also to realize millimetre-scale SPAD arrays with low dark counts and minimal crosstalk<sup>45</sup>. The silicon photomultiplier device — an array of SPAD pixels that are read in parallel — can

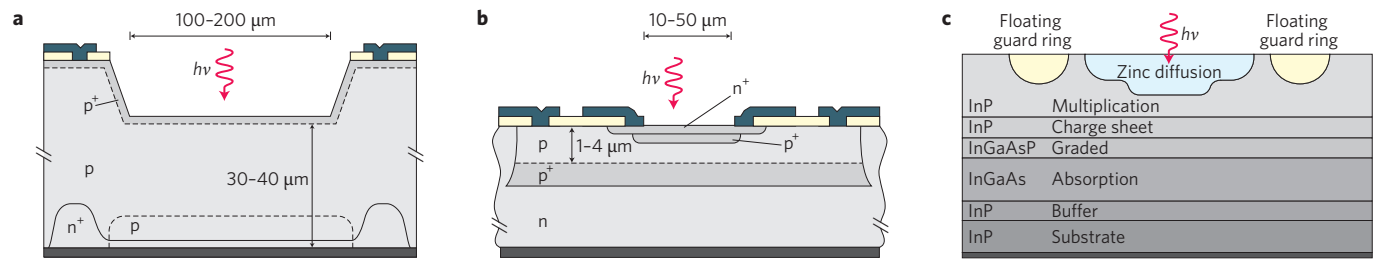


**Figure 3 | Established photon-counting technologies based on reverse-biased avalanche photodiodes.** **a**, Thick-junction Si SPAD, a device structure optimized for high detection efficiency and low dark counts. **b**, Shallow-junction planar Si SPAD, a device structure optimized for low timing jitter requiring low bias voltages. **c**, InGaAs/InP SPAD structure, where the use of a smaller-bandgap semiconductor extends single-photon sensitivity to telecommunications wavelengths. Figures reproduced with permission from: **a,b**, ref. 43, © 2004 Taylor & Francis; **c**, ref. 52, © 2006 IEEE.

offer extremely high count rates ( $\sim 400$  MHz) and photon number resolution, but suffer from elevated dark counts<sup>46</sup>.

To extend the performance of SPADs to telecommunications wavelengths ( $\lambda = 1,310$  nm and 1,550 nm) it is necessary to use lower-bandgap semiconductor materials such as Ge and InGaAs. The best results have been achieved with an InGaAs absorption region and an InP multiplication layer, giving single-photon sensitivities across the 1,000–1,600 nm wavelength range and peak efficiencies of  $\sim 20\%$  at 1,550 nm (refs 47–52). The diameter of the active device is  $\sim 40$   $\mu\text{m}$ , which is suitable for fibre coupling. Owing to materials defects, these devices suffer from dark count rates that are orders of magnitude higher than for their Si counterparts. As a result, InGaAs SPADs are typically operated in gated Geiger mode<sup>51</sup> — the quiescent device is biased beneath the breakdown voltage, then a short ( $\sim 1$  ns) pulse is applied, coincident with the expected arrival of a photon. The dark count rate can be reduced to  $\sim 10$  kHz (including gating) by cooling to  $\sim 200$  K, but this reduction in temperature exacerbates afterpulsing, causing long detector dead times of around 10  $\mu\text{s}$  and reducing counting rates to  $\sim 100$  kHz. These devices are now commercially available<sup>53,54</sup> and have allowed fibre QKD systems to reach distances beyond 100 km (ref. 55).

Much of the ongoing effort to improve InGaAs SPAD performance is targeted at QI applications such as QKD. Imaginative biasing and gating schemes, combined with higher-temperature operating schemes to reduce afterpulsing, have led to increased device clock rates<sup>56–58</sup>, thus increasing overall bit-rates in QKD<sup>57</sup>. It is also possible to extract multiphoton sensitivity through such methods<sup>59</sup>. Passive quenching at low excess bias can enable free-running operation<sup>60</sup>. Looking ahead, SPADs based on new materials systems such as HgCdTe (ref. 61) may lead to improved long-wavelength performance.

### Emerging single-photon detector technologies

We now review a selection of the most promising emerging single-photon detector technologies under consideration for use in QI applications. The operating principle, performance, advantages and disadvantages of each detector are detailed. Where possible, the properties of each emerging technology are compared with those of the established single-photon detector types in Table 1. Instances where these emerging technologies have been implemented in optical QI experiments are highlighted. Recent developments and the potential for future improvements of these technologies are also discussed.

**Frequency up-conversion.** The goal of frequency up-conversion single-photon detection schemes is to convert a telecommunications-wavelength photon to a shorter wavelength that can be more efficiently detected by a commercial single-photon detector. An example of such a scheme is illustrated in Fig. 4a. The mechanism used is sum-frequency generation in a nonlinear optical crystal: a weak signal at frequency  $\omega_{\text{in}}$  is combined with a strong pump signal

at frequency  $\omega_{\text{pump}}$  to yield an output signal at the summation frequency of  $\omega_{\text{out}} = \omega_{\text{in}} + \omega_{\text{pump}}$ . If sufficient pump power is available, this frequency up-conversion can occur with near-unity efficiency. For example, in periodically poled lithium niobate, using a pump signal at 1,064 nm allows 1,550-nm photons to be converted to 630-nm photons with 90% efficiency<sup>62</sup>. There are several technical challenges in achieving high-efficiency up-conversion. The first is to achieve the desired field strength, either through a coincident pump and signal pulse<sup>63</sup>, a continuous-wave pump pulse and a build up cavity<sup>62</sup>, or by using a waveguide to concentrate the pump power into a small interaction region<sup>64</sup>. Drawbacks include the difficulty of stabilizing the nonlinear crystal, the presence of nonlinear processes that lead to fluorescence at the up-conversion wavelength (resulting in very high background count rates), and high in- and output coupling losses for waveguides. Up-conversion schemes using thick-junction Si SPADs have shown system detection efficiencies of 46% for 1,550-nm photons, with a jitter of 400-ps at FWHM and dark count rates of 800 kHz (ref. 65). Shallow-junction Si SPADs have also been used, achieving a system detection efficiency of 2% at 1,550 nm, a FWHM jitter of 40 ps and a dark count rate of 20 kHz (ref. 66). Low-jitter hybrid photodetectors have also been used in conjunction with up-conversion<sup>67</sup>. All three variants have been implemented in QKD demonstrations<sup>65–67</sup>. Recent studies have also shown that coherent up-conversion of quantum states is feasible<sup>68</sup>, which is an important step for advanced QI applications.

**Visible-light photon counters.** The visible-light photon counter (VLPC) is a low-temperature semiconductor-based photon counting technology<sup>69–71</sup>. The device offers high-efficiency detection of single photons up to wavelengths of 1  $\mu\text{m}$ , the ability to resolve photon number, good timing resolution and moderate dark counts.

The VLPC is based on an earlier concept called the solid-state photomultiplier, a blocked-impurity-band device based on As-doped silicon, which gives single-photon sensitivity from visible wavelengths up to 30  $\mu\text{m}$ . Solid-state photomultiplier and VLPC devices operate at low voltage through a controlled single-carrier multiplication process, giving rise to a signal that is proportional to the photon number. In a VLPC the gain region and absorber are separate, maximizing the sensitivity in the wavelength range of 400–1,000 nm. A schematic of the device architecture is shown in Fig. 4b. An electron–hole pair is generated in the undoped (intrinsic) Si absorber region, and the resulting hole triggers an avalanche in the gain region through interaction with As impurity levels. This single-carrier multiplication process only requires a small bias voltage of 6–7.5 V, but the device temperature must be carefully tuned to around 6 K to achieve optimal performance. As the avalanche is confined to a 20- $\mu\text{m}$ -wide filament and the overall device diameter is 1 mm, two photons can produce distinct concurrent avalanches if the focal spot is large. The low excess noise of the multiplication

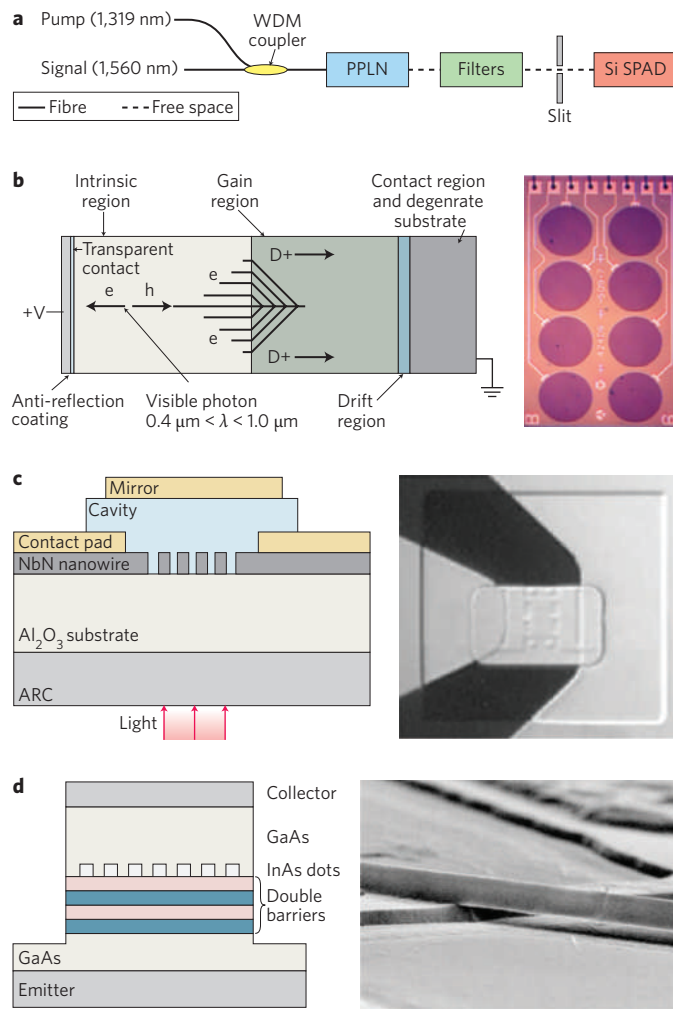


**Figure 4 | Emerging single-photon detectors: a selection of promising technologies.** **a**, Frequency up-conversion detector. A 1,560-nm photon is converted to a 715-nm photon through sum frequency generation in a periodically poled lithium niobate waveguide, and is detected by a Si SPAD. WDM, wavelength-division multiplexer. **b**, Visible-light photon counter. This is a low-temperature semiconductor technology. The single-carrier multiplication process allows for photon number resolution. A device schematic (left) and an optical micrograph of eight VLPC pixels (right) are shown. **c**, A next-generation superconducting nanowire single-photon detector, showing the device schematic (left) and optical micrograph (right). A niobium nitride (NbN) SNSPD is embedded in a resonant cavity to enhance the detection efficiency. ARC, anti-reflection coating. **d**, A detector based on a quantum dot resonant tunnelling diode, showing the device schematic (left) and a scanning electron micrograph of the cross-wire device structure (right). Figures reproduced with permission from: **a**, ref. 65, © 2005 IOP; **b**, ref. 71, © 2003 IEEE; **c**, ref. 87, © 2005 OSA; **d**, ref. 96, © 2005 APS.

process is close to the theoretical minimum, allowing up to five photons to be resolved<sup>70,71</sup>. VLPC detection efficiencies of up to 88% at 694 nm and 93% in the infrared have been observed, neglecting coupling losses and spectral filtering<sup>69</sup>. The dark count rate is ~20 kHz at the maximum detection efficiency. The dead time of the VLPC is ~100 ns, and therefore the upper limit to the count rate is ~100 kHz. The jitter of these devices has recently been measured at 633 nm (unpublished data, Burm Baek, NIST, USA, 2009), and the lowest value obtained is 250 ps at FWHM in the dark count

range of 6.9–25 kHz, with a maximum fibre-coupled detection efficiency of 40%.

VLPCs are highly desirable for QI applications requiring high detection efficiency and photon number resolution. So far, VLPCs have been successfully used in studies of photon statistics in non-classical parametric down-conversion sources<sup>72</sup>.

**Superconducting transition-edge sensors.** Superconducting transition-edge sensors (TESs) are low-temperature devices that offer very-high-efficiency single-photon detection with photon-number-resolving capability and low dark count rates. In a TES, the detector element is a superconducting film on the cusp of the superconducting transition, where any change in temperature will cause an abrupt change in resistance<sup>73</sup>. The absorption of an incident photon heats the device, causing the voltage-biased detector to draw a current that can be read out using a SQUID amplifier. The signal is proportional to the energy of the photon or, at fixed wavelength, the photon number<sup>74</sup>. This intrinsic ability to resolve photon number is illustrated in Fig. 2a<sup>20</sup>. These detectors operate at temperatures of around 100 mK and therefore require sophisticated cooling technology. The current tungsten-based detectors have a detection efficiency of 20%<sup>75</sup> — which increases to 95% efficiency at 1,550 nm (ref. 20) when they are embedded in an optical cavity structure — and have negligible dark counts. In practical implementations, the effective dark count rate may rise due to room-temperature black-body radiation<sup>76</sup>. This effect can be mitigated by filtering, but this reduces the detection efficiency. The photon-number-resolving capabilities are excellent — up to eight photons can be resolved clearly<sup>20</sup>. High-efficiency devices for the near-infrared (~850 nm) have also recently been reported<sup>77</sup>. The timing properties of TES detectors are relatively poor, with jitter times of around 100 ns at FWHM. The dead time of the detector is limited by the thermal time constant of the detector element, and is typically ~1 μs. Faster detectors, with dead times around 100 ns, can be fabricated using films of higher transition temperatures<sup>77</sup>, but these devices require faster SQUID read-out electronics.

TES detectors have so far been successfully implemented in quantum optics experiments<sup>78</sup> and long-distance QKD<sup>76,79</sup>. Owing to their near-unity detection efficiency and ability to resolve photon number, these detectors are highly promising candidates for fundamental tests of quantum mechanics, LOQC and optical quantum metrology applications.

**Superconducting nanowire single-photon detectors** Superconducting nanowire single-photon detectors (SNSPDs) offer single-photon sensitivity from visible to mid-infrared wavelengths, low dark counts, short recovery times and low timing jitter.

The detector element itself is a 100-nm-wide nanowire that is patterned by electron-beam lithography in an ultrathin niobium nitride superconducting film<sup>80</sup>. It operates in the temperature range of 1.5–4 K, well below the superconducting transition temperature of the niobium nitride film. The material is chosen because of its exceptionally fast photoresponsive properties<sup>81</sup>. The superconducting wire is biased just below its critical current, which is the point at which the wire becomes resistive. When a photon strikes the wire, a local resistive hotspot is formed, perturbing the current distribution and thus triggering a fast voltage-pulse<sup>80</sup> that can then be amplified and measured. The detection efficiency and dark count rate are both dependent on the bias point, with the dark count rate rising more steeply close to the critical current.

Current devices consist of a ‘meander wire’<sup>82</sup> that covers an area of up to 20 μm × 20 μm (ref. 83) to achieve a high coupling efficiency between the nanowire and a single-mode optical fibre. The device is embedded in a microwave coplanar waveguide to facilitate the read-out of fast voltage pulses. Fabrication of large-area detectors is challenging

because the wire must be completely uniform along its length — a constriction at any point in the wire will negate the sensitivity of the rest of the detector<sup>84</sup>. The use of a single, long meander wire increases the overall inductance, lengthening the detector dead time<sup>85</sup> to around 10 ns for large-area detectors<sup>86</sup> — although this is a significant increase, it is still an order of magnitude faster than conventional photon counters. The intrinsic efficiency of small-area ( $3\ \mu\text{m} \times 3.3\ \mu\text{m}$ ) single-layer SNSPDs is as high as 20% at 1,550 nm, which is close to the expected absorption of the material<sup>87</sup>. Fibre-coupled large-area SNSPDs offer practical detection efficiencies of  $>1\%$  at 1,550 nm, with dark count rates below 1 kHz (refs 83,86). The timing jitter of the device is extremely good (compared with Si SPADs<sup>16</sup>; Fig. 1b) — 65 ps at FWHM can be achieved in large-area devices<sup>19</sup>, and 30 ps FWHM or less in small-area devices<sup>87</sup>.

An exciting aspect of this technology is that considerable performance improvements are well within reach. SNSPDs have been integrated into low-Q optical cavity structures with back-reflector mirrors (the device architecture and an optical micrograph are shown in Fig. 4c). This improves the intrinsic detection efficiency to as much as 57% for small-area devices<sup>87</sup>. The addition of a cavity does not degrade the timing performance of the detector. A limitation of current niobium nitride devices is that they must be grown on lattice-matched substrates (sapphire or MgO) at high temperatures ( $>600\ \text{°C}$ ). The demonstration of high-quality devices on alternative substrates, such as NbTiN deposited at room temperature on Si (ref. 88), will increase the versatility of this detector technology. Multipixel SNSPD devices have also recently been demonstrated<sup>120,89</sup>. Such devices provide spatially multiplexed photon number resolution, allowing larger detector areas to be achieved with both low timing jitter and short recovery times.

Basic meander-type SNSPDs<sup>82</sup> have now been widely implemented in optical QI applications. Fibre-coupled SNSPDs can be integrated into practical, closed-cycle refrigerator systems operating at  $\sim 3\ \text{K}$  (ref. 86), widening the range of accessible applications. SNSPDs have had a major impact in the field of QKD, leading to record transmission distances and bit-rates in optical fibres<sup>90</sup>. As next-generation high-efficiency devices<sup>87</sup> become available, the importance of these detectors in optical QI science and technology is expected to continue increasing.

**Single-photon detectors based on quantum dots and semiconductor defects.** Another new class of devices utilize the trapping of charge in defects to achieve single-photon detection. Semiconductor heterostructures based on III–V compounds form the basic device architecture: either quantum dots (QDs) embedded in the material<sup>91–97</sup> or intrinsic defects<sup>98</sup> are exploited to achieve trapping. QDs are favoured as they can be controllably placed within the heterostructure to maximize internal efficiency and signal uniformity. Two main detection schemes have been realized. The first relies on a photoconductive gain mechanism that involves trapping charge in a defect or QD layer, which alters the conductance in a field-effect transistor structure<sup>91–95,98</sup>. These types of device have been operated at count rates of up to 400 kHz (ref. 92), and a high internal efficiency of up to 68% has been demonstrated at 805 nm (ref. 93). Resolution of up to three photons in such devices has also been shown<sup>94,95</sup>.

The second scheme relies on photo-absorption in a QD, which alters the tunnelling probability in a resonant tunnel diode structure<sup>96,97</sup>. Quantum-dot-resonant tunnel diode devices have demonstrated single-photon detection efficiencies of up to 12% at 550 nm, jitter of 150 ns and very low dark count rates (down to  $2 \times 10^{-3}\ \text{Hz}$ ). Devices of this type have recently been realized at telecommunications wavelengths<sup>97</sup>.

These devices are currently at an early stage of development; the only successful demonstrations have been carried out at cryogenic temperatures ( $\sim 4\ \text{K}$ ). Low dark count rates have been reported.

Device performance seems to be limited by large timing jitter, and practical detection efficiencies are low because of the micrometre-scale device areas. Improvements are anticipated, however, and if sources of noise can be eliminated, higher temperature operation may be possible. Furthermore, resonant cavities may boost device efficiency. This class of detectors offers intriguing prospects for future QIP technologies. There is a clear compatibility with III–V semiconductor QD single-photon sources<sup>19</sup>. There is also potential for these types of structures to achieve spin-preserving photodetection<sup>99</sup>; transferring photon polarization to electron or hole spin is one possible candidate for emerging quantum memory and repeater technologies.

## Outlook and conclusion

This review has summarized key performance parameters and defined a figure of merit for single-photon detectors in optical quantum information applications. The current performance of established and emerging detector technologies has also been reviewed. Semiconductor-based detectors such as single-photon avalanche diodes have attained a high level of maturity and are widely used in laboratory quantum optics and quantum information experiments. There are ongoing efforts to improve the performance of single-photon avalanche diodes at telecommunications wavelengths, for quantum information applications such as long-distance quantum key distribution in optical fibre. To meet the demands of new quantum information applications, a host of new single-photon detector technologies are being rapidly devised, developed, evaluated and deployed. As a result, low-temperature detectors with infrared sensitivity, excellent timing resolution and a high signal-to-noise ratio, such as superconducting nanowire single-photon detectors, have set new benchmarks in long distance, high-bit-rate quantum key distribution. Visible-light photon counters and superconducting transition-edge sensors now offer near-unity detection efficiency and the ability to resolve photon number, which are both prerequisites for scalable linear optical quantum computing. These improvements in detector technology are therefore having an immediate scientific impact, allowing the frontiers of quantum information science and quantum optics to be pushed forward. Moreover, these new single-photon detector technologies are poised to have a profound impact in a range of fields far beyond that of quantum information. There is widespread demand for improved single-photon detectors, particularly at infrared wavelengths; such technologies are eagerly awaited in fields as diverse as astronomy, laser ranging, remote sensing, classical communications and biomedical imaging.

## References

1. Einstein, A. On a heuristic point of view about the creation and conversion of light. *Ann. Phys. (Leipz.)* **17**, 132–148 (1905).
2. Loudon, R. *Quantum Theory of Light* 3rd edn, Ch. 1 (Oxford Univ. Press, 2000).
3. Becker, W. *Advanced Time-Correlated Single Photon Counting Techniques* Ch. 2 (Springer, 2005).
4. Migdall, A. Introduction to journal of modern optics special issue on single-photon: detectors, applications, and measurement methods. *J. Mod. Opt.* **51**, 1265–1266 (2004).
5. Nielsen, M. A. & Chuang, I. L. *Quantum Computation and Quantum Information* Ch. 1 (Cambridge Univ. Press, 2000).
6. Zoller, P. *et al.* Quantum information processing and communication. *Eur. Phys. J. D* **36**, 203–228 (2005).
7. Bennett, C. H. & Brassard, G. in *Proc. IEEE Int. Conf. Computers, Systems and Signal Processing, Bangalore* 175–179 (1984).
8. Gisin, N., Ribordy, G., Tittel, W. & Zbinden, H. Quantum cryptography. *Rev. Mod. Phys.* **74**, 145–195 (2002).
9. Knill, E., Laflamme, R. & Milburn, G. J. A scheme for efficient quantum computation with linear optics. *Nature* **409**, 46–52 (2001).
10. Kok, P. *et al.* Linear optical quantum computing with photonic qubits. *Rev. Mod. Phys.* **79**, 135–175 (2007).
11. O'Brien, J. L. Optical quantum computing. *Science* **318**, 1567–1570 (2007).

12. Varnava, M., Browne, D. E. & Rudolph, T. How good must single photon sources and detectors be for efficient linear optical quantum computation? *Phys. Rev. Lett.* **100**, 060502 (2008).
13. Bachor, H.-A. & Ralph, T. C. A *Guide to Experiments in Quantum Optics* 2nd edn, Ch. 7 (Wiley-VCH, 2004).
14. Rarity, J. G., Ridley, K. D. & Tapster, P. R. Absolute measurement of detector quantum efficiency using parametric downconversion. *Appl. Opt.* **26**, 4616–4619 (1987).
15. Ware, M. & Migdall, A. Single-photon detector characterization using correlated photons: the march from feasibility to metrology. *J. Mod. Opt.* **51**, 1549–1557 (2004).
16. Stevens, M. J. *et al.* Fast lifetime measurements of infrared emitters using a low-jitter superconducting single-photon detector. *Appl. Phys. Lett.* **89**, 031109 (2006).
17. Silberhorn, C. Detecting quantum light. *Contemp. Phys.* **48**, 143–156 (2007).
18. Kumar, P. *et al.* Photonic technologies for quantum information processing. *Quantum Inf. Process.* **3**, 215–231 (2004).
19. Shields, A. J. Semiconductor quantum light sources. *Nature Photon.* **1**, 215–223 (2007).
20. Lita, A. E., Miller, A. J. & Nam, S. W. Counting near-infrared single-photons with 95% efficiency. *Opt. Express* **16**, 3032–3040 (2008).
21. Jiang, L. A., Dauber, E. A. & Chang, J. T. Photon-number-resolving detector with 10 bits of resolution. *Phys. Rev. A* **75**, 062325 (2007).
22. Divochiy, A. *et al.* Superconducting nanowire photon-number-resolving detector at telecommunication wavelengths. *Nature Photon.* **2**, 302–306 (2008).
23. Achilles, D., Silberhorn, C., Sliwa, C., Banaszek, K. & Walmsley, I. A. Fiber-assisted detection with photon-number resolution. *Opt. Lett.* **28**, 2387–2389 (2003).
24. Donati, S. *Photodetectors: Devices, Circuits and Applications* Ch. 3 (Prentice Hall, 2000).
25. Cheung, J., Migdall, A. & Rastello, M.-L. Single-photon sources, detectors, applications and measurement methods. *J. Mod. Opt.* **56**, 139–140 (2009).
26. Morton, G. A. Photomultipliers for scintillation counting. *RCA Rev.* **10**, 525–553 (1949).
27. Poultney, S. K. Single-photon detection and timing: experiments and techniques. *Adv. Electron. El. Phys.* **31**, 39–117 (1972).
28. <http://jp.hamamatsu.com/>.
29. <http://www.burle.com/index.html>.
30. Kume, H., Koyama, K., Nakatsugawa, K., Suzuki, S. & Fatlowitz, D. Ultrafast microchannel plate photomultipliers. *Appl. Opt.* **27**, 1170–1178 (1988).
31. <http://jp.hamamatsu.com/resources/products/etd/pdf/m-h7422e.pdf>.
32. [http://jp.hamamatsu.com/resources/products/etd/pdf/NIR-PMT\\_APPLI\\_TPMO1040E02.pdf](http://jp.hamamatsu.com/resources/products/etd/pdf/NIR-PMT_APPLI_TPMO1040E02.pdf).
33. Fukasawa, A., Haba, J., Kageyama, A., Nakazawa, H. & Suyama, M. High speed HPD for photon counting. *IEEE Trans. Nucl. Sci.* **55**, 758–762 (2008).
34. Cova, S., Longoni, A. & Andreoni, A. Towards picoseconds resolution with single-photon avalanche diodes. *Rev. Sci. Instr.* **52**, 408–412 (1981).
35. Haitz, R. H. Mechanisms contributing to the noise pulse rate of avalanche diodes. *J. Appl. Phys.* **36**, 3123–3131 (1965).
36. Brown, R. G. W., Jones, R., Rarity, J. G. & Ridley, K. D. Characterization of silicon avalanche photodiodes for photon correlation measurements 2: Active quenching. *Appl. Opt.* **26**, 2383–2389 (1987).
37. Daudet, H. *et al.* Photon counting techniques with silicon avalanche photodiodes. *Appl. Opt.* **32**, 3894–3900 (1993).
38. [http://optoelectronics.perkinelmer.com/content/RelatedLinks/SpecificationSheets/SPC\\_PhotoDetectors.pdf](http://optoelectronics.perkinelmer.com/content/RelatedLinks/SpecificationSheets/SPC_PhotoDetectors.pdf).
39. Blazej, J. Photon number resolving in Geiger mode avalanche photodiode photon counters. *J. Mod. Opt.* **51**, 1491–1498 (2004).
40. Kurtsiefer, C., Zarda, P., Mayer, S. & Weinfurter, H. The breakdown flash of silicon avalanche photodiodes — a back door for eavesdropper attacks? *J. Mod. Opt.* **48**, 2039–2047 (2001).
41. [http://www.microphotondevices.com/products\\_pdm.asp](http://www.microphotondevices.com/products_pdm.asp).
42. Cova, S., Lacaita, A., Ghioni, M., Ripamonti, G. & Louis, T. A. 20-ps timing resolution with single-photon avalanche diodes. *Rev. Sci. Instr.* **60**, 1104–1110 (1989).
43. Cova, S., Ghioni, M., Lotito, A., Rech, I. & Zappa, F. Evolution and prospects for single-photon avalanche diodes and quenching circuits. *J. Mod. Opt.* **51**, 1267–1288 (2004).
44. Zappa, F., Ghioni, M., Cova, S., Samori, C. & Giudice, A. C. An integrated active-quenching circuit for single-photon avalanche diodes. *IEEE Trans. Instr. Meas.* **49**, 1167–1175 (2000).
45. Rech, I. *et al.* Optical crosstalk in single photon avalanche diode arrays: a new complete model. *Opt. Express* **16**, 8381–8394 (2008).
46. Eraerds, P., Legré, M., Rochas, A., Zbinden, H. & Gisin, N. SiPM for fast photon-counting and multiphoton detection. *Opt. Express* **15**, 14539–14549 (2007).
47. Lacaita, A., Zappa, F., Cova, S. & Lovati, P. Single-photon detection beyond 1  $\mu\text{m}$ : performance of commercially available InGaAs/InP detectors. *Appl. Opt.* **35**, 2986–2996 (1996).
48. Ribordy, G., Gautier, J.-D., Zbinden, H. & Gisin, N. Performance of InGaAs/InP avalanche photodiodes as gated-mode photon counters. *Appl. Opt.* **37**, 2272–2277 (1998).
49. Rarity, J. G., Wall, T. E., Ridley, K. D., Owens, P. C. M. & Tapster, P. R. Single-photon counting for the 1300–1600-nm range by use of Peltier-cooled and passively quenched InGaAs avalanche photodiodes. *Appl. Opt.* **39**, 6746–6753 (2000).
50. Hiskett, P. A. *et al.* Performance and design of InGaAs/InP photodiodes for single-photon counting at 1.55  $\mu\text{m}$ . *Appl. Opt.* **39**, 6818–6829 (2000).
51. Bethune, D. S. & Risk, W. P. An autocompensating fiber-optic quantum cryptography system based on polarization splitting of light. *IEEE J. Quant. Elect.* **36**, 340–347 (2000).
52. Pellegrini, S. *et al.* Design and performance of an InGaAs-InP single-photon avalanche diode detector. *IEEE J. Quant. Elect.* **42**, 397–403 (2006).
53. <http://www.princetonlightwave.com/content/PGA-400%20V1.0.pdf>.
54. <http://www.idquantique.com/products/files/id201-specs.pdf>.
55. Gobby, C., Yuan, Z. L. & Shields, A. J. Quantum key distribution over 122 km of standard telecom fiber. *Appl. Phys. Lett.* **84**, 3762–3764 (2004).
56. Namekata, N., Sasamori, S. & Inoue, S. 800 MHz single-photon detection at 1550-nm using an InGaAs/InP photodiode operated with a sine wave gating. *Opt. Express* **14**, 10043–10049 (2006).
57. Dixon, A. R., Yuan, Z. L., Dynes, J. F., Sharpe, A. W. & Shields, A. J. Gigahertz decoy quantum key distribution with 1 Mbit/s secure key rate. *Opt. Express* **16**, 18790–18797 (2008).
58. Thew, R. T., Stucki, D., Gautier, J.-D., Zbinden, H. & Rochas, A. Free-running InGaAs/InP avalanche photodiode with active quenching for single photon counting at telecom wavelengths. *Appl. Phys. Lett.* **91**, 201114 (2007).
59. Kardynał, B. E., Yuan, Z. L. & Shields, A. J. An avalanche-photodiode-based photon-number-resolving detector. *Nature Photon.* **2**, 425–428 (2008).
60. Warburton, R. E., Itzler, M. & Buller, G. S. Free-running room temperature operation of an InGaAs/InP single-photon avalanche diode. *Appl. Phys. Lett.* **94**, 071116 (2009).
61. Rogalski, A., Antoszewski, J. & Faraone, L. Third-generation infrared photodetector arrays. *J. Appl. Phys.* **105**, 091101 (2009).
62. Albota, M. A. & Wong, F. N. C. Efficient single-photon counting at 1.55  $\mu\text{m}$  by means of frequency upconversion. *Opt. Lett.* **29**, 1449–1451 (2004).
63. Vandevender, A. P. & Kwiat, P. G. High efficiency single-photon detection via frequency up-conversion. *J. Mod. Opt.* **51**, 1433–1445 (2004).
64. Langrock, C. *et al.* Highly efficient single-photon detection at communication wavelengths by use of upconversion in reverse-proton exchanged periodically poled LiNbO<sub>3</sub> waveguides. *Opt. Lett.* **30**, 1725–1727 (2005).
65. Takesue, H. *et al.* Differential phase shift quantum key distribution experiment over 105 km fibre. *New J. Phys.* **7**, 232–243 (2005).
66. Thew, R. T. *et al.* Low jitter up-conversion detectors for telecom wavelength GHz QKD. *New J. Phys.* **8**, 32–43 (2006).
67. Zhang, Q. *et al.* Megabits secure key rate quantum key distribution. *New J. Phys.* **11**, 045010 (2009).
68. Tanzilli, S. *et al.* A photonic quantum information interface. *Nature* **437**, 116–120 (2005).
69. Takeuchi, S., Kim, J., Yamamoto, Y. & Hogue, H. H. Development of a high-quantum-efficiency single-photon counting system. *Appl. Phys. Lett.* **74**, 1063–1065 (1999).
70. Kim, J., Takeuchi, S., Yamamoto, Y. & Hogue, H. H. Multiphoton detection using visible light photon counter. *Appl. Phys. Lett.* **74**, 902–904 (1999).
71. Waks, E. *et al.* High-efficiency photon-number detection for quantum information processing. *IEEE J. Sel. Top. Quant.* **9**, 1502–1511 (2003).
72. Waks, E., Diamanti, E., Sanders, B. C., Bartlett, S. D. & Yamamoto, Y. Direct observation of nonclassical photon statistics in parametric down-conversion. *Phys. Rev. Lett.* **92**, 113602 (2004).
73. Cabrera, B. *et al.* Detection of single infrared, optical and ultraviolet photons using superconducting transition edge sensors. *Appl. Phys. Lett.* **73**, 735–737 (1998).
74. Miller, A. J., Nam, S. W., Martinis, J. M. & Sergienko, A. V. Demonstration of a low-noise near-infrared photon counter with multiphoton discrimination. *Appl. Phys. Lett.* **83**, 791–793 (2003).
75. Rosenberg, D., Lita, A. E., Miller, A. J. & Nam, S. W. Noise-free high-efficiency photon-number-resolving detectors. *Phys. Rev. A* **71**, 061803 (2005).
76. Rosenberg, D. *et al.* Long-distance decoy-state quantum key distribution in optical fiber. *Phys. Rev. Lett.* **98**, 010503 (2007).
77. Fukuda, D. *et al.* Photon number resolving detection with high speed and high quantum efficiency. *Metrologia* **46**, S288–S292 (2009).
78. Di Giuseppe, G. *et al.* Direct observation of photon pairs at a single output port of a beam-splitter interferometer. *Phys. Rev. A* **68**, 063817 (2003).

79. Rosenberg, D. *et al.* Quantum key distribution at telecom wavelengths with noise-free detectors. *Appl. Phys. Lett.* **88**, 021108 (2006).
80. Gol'tsman, G. N. *et al.* Picosecond superconducting single-photon optical detector. *Appl. Phys. Lett.* **79**, 705–707 (2001).
81. Il'in, K. S. *et al.* Picosecond hot-electron energy relaxation in NbN superconducting photodetectors. *Appl. Phys. Lett.* **76**, 2752–2754 (2000).
82. Verevkin, A. *et al.* Detection efficiency of large-active-area NbN single-photon superconducting detectors in the ultraviolet to near-infrared range. *Appl. Phys. Lett.* **80**, 4687–4689 (2002).
83. Miki, S. *et al.* Large sensitive-area NbN nanowire superconducting single-photon detectors fabricated on single-crystal MgO substrates. *Appl. Phys. Lett.* **92**, 061116 (2008).
84. Kerman, A. J. *et al.* Constriction-limited detection efficiency of superconducting nanowire single-photon detectors. *Appl. Phys. Lett.* **90**, 101110 (2007).
85. Kerman, A. J. *et al.* Kinetic-inductance-limited reset time of superconducting nanowire photon counters. *Appl. Phys. Lett.* **88**, 111116 (2006).
86. Hadfield, R. H. *et al.* Single photon source characterization with a superconducting single photon detector. *Opt. Express* **13**, 10846–10853 (2005).
87. Rosfjord, K. M. *et al.* Nanowire single-photon detector with an integrated optical cavity and anti-reflection coating. *Opt. Express* **14**, 527–534 (2006).
88. Dorenbos, S. N. *et al.* Low noise superconducting single photon detectors on silicon. *Appl. Phys. Lett.* **93**, 131101 (2008).
89. Dauler, E. A. *et al.* Photon-number-resolution with sub-30-ps timing using multi-element superconducting nanowire single photon detectors. *J. Mod. Opt.* **56**, 364–373 (2009).
90. Takesue, H. *et al.* Quantum key distribution over 40-dB channel loss using superconducting single-photon detectors. *Nature Photon.* **1**, 343–348 (2007).
91. Shields, A. J. *et al.* Detection of single photons using a field-effect transistor gated by a layer of quantum dots. *Appl. Phys. Lett.* **76**, 3673–3675 (2000).
92. Kardynał, B. E. *et al.* Low-noise photon counting with a radio-frequency quantum-dot field-effect transistor. *Appl. Phys. Lett.* **84**, 419–421 (2004).
93. Rowe, M. A. *et al.* Single-photon detection using a quantum dot optically gated field-effect transistor with high internal quantum efficiency. *Appl. Phys. Lett.* **89**, 253505 (2006).
94. Kardynał, B. E. *et al.* Photon number resolving detector based on a quantum dot field effect transistor. *Appl. Phys. Lett.* **90**, 181114 (2007).
95. Gansen, E. J. *et al.* Photon-number-discriminating detection using a quantum-dot, optically gated, field-effect transistor. *Nature Photon.* **1**, 585–588 (2007).
96. Blakesley, J. C. *et al.* Efficient single photon detection by quantum dot resonant tunneling diodes. *Phys. Rev. Lett.* **94**, 067401 (2005).
97. Li, H. W. *et al.* Quantum dot resonant tunneling diode for telecommunication wavelength single photon detection. *Appl. Phys. Lett.* **91**, 073516 (2007).
98. Kosaka, H. *et al.* Photoconduction quantization in a single-photon detector. *Phys. Rev. B* **65**, 201307 (2002).
99. Yablonoivitch, E. *et al.* Optoelectronic quantum telecommunications based on spins in semiconductors. *Proc. IEEE* **91**, 761–780 (2003).

### Acknowledgements

R.H.H. thanks colleagues at NIST, Boulder, USA, and Heriot-Watt University, Edinburgh, UK, for helpful discussions and comments. He also thanks colleagues who provided figures for the manuscript. His work is supported by the Royal Society of London through a University Research Fellowship and the UK Engineering and Physical Sciences Research Council.